(Received 2 March 2025, Accepted 14 May 2025, Scheduled 24 May 2025)

A Compact 4 x 4 UWB MIMO Antenna with 5G and WLAN Band Rejected Operation

Lei He, Youming Miao, and Gui Liu*

College of Electrical and Electronic Engineering, Wenzhou University, Wenzhou 325035, China

ABSTRACT: An ultra-compact four-port ultra-wideband (UWB) antenna with dual notches is designed to reject the 5G (3.3–4.2 GHz, 4.8–5 GHz) and WLAN (5.15–5.825 GHz) frequency bands. The proposed antenna consists of four orthogonal antenna elements and some defected ground planes. A double T-shaped filter structure is employed on the radiation unit, which generates a notch frequency band of 3.3–4.2 GHz. Additionally, a complementary split resonant ring (CSRR) structure is created on the ground plane to suppress the frequency band from 4.8 GHz to 6 GHz by adjusting the size and position of the slots. The measured −10 dB impedance bands are 4.2–4.8 GHz and 6.0–11.0 GHz. The isolation performance exceeds 17 dB across the operational bandwidth. Furthermore, the envelope correlation coefficient (ECC) remains consistently below 0.03 within the 4.2–4.8 GHz and 6.0–11.0 GHz range. Within the operational band, the efficiency values range between 70.7% and 92.4%. The proposed antenna is applicable in civil communication, military, and medical fields.

1. INTRODUCTION

Since the frequency of ultra-wideband (UWB) was confirmed and opened to the field of civil communications, UWB communication technology has received extensive attention. A UWB system is characterized by its ultra-wideband capabilities and high-speed data transmission. However, a UWB system faces the challenges of reliability and multipath fading, which are critical in personal area network applications [1]. Additionally, without multiple antennas for beamforming, the coverage and signal quality at the network edges may be compromised. Multiple-input multiple-output (MIMO) has been identified as a promising approach to addressing wireless communication system challenges [2].

MIMO technology is indispensable to communication systems for its significant advantages, and it significantly improves system capacity and data throughput through spatial multiplexing gain, enabling wireless communication systems to transmit more information under the same spectrum resources [3]. Furthermore, spatial diversity gain provides a strong guarantee for the robustness of the signal and effectively reduces the impact of multipath fading and external interference on communication quality [4]. In addition, the beamforming function of MIMO technology also has great practical value. By adjusting the phase and amplitude of the antenna array, the signal energy can be concentrated in a certain direction, thereby expanding the coverage of the signal and optimizing the user experience at the edge of the network. This feature is significant for improving the coverage quality and user satisfaction of wireless networks [5]. Additionally, MIMO technology plays a key role in improving spectrum efficiency. Not only does it not need to add more spectrum but also makes the system more flexible and scalable, laying a solid foundation for future wireless communication [6].

One of the key challenges in designing MIMO antennas is to minimize coupling between antennas. As antennas become miniaturized and the distance between antenna units decreases, problems of mutual coupling and electromagnetic interference become more severe. Therefore, improving antenna isolation has become a core research goal in the development of MIMO systems. By optimizing antenna layout, adopting new materials and design techniques, researchers are working to solve this problem in order to achieve higher isolation and smaller size while maintaining antenna performance [7, 8]. Progress in this research direction will provide strong support for enhancing the performance and promoting the widespread application of wireless communication systems.

Numerous strategies have been explored to enhance isolation within MIMO antenna configurations, including the implementation of decoupling structures [9], the integration of neutral lines [10–12], the introduction of opening slits [13], the application of electromagnetic bandgap (EBG) structures [14–16], the adoption of polarization diversity technology [17, 18], and the utilization of defective ground structures [19, 20]. In [9], the researchers detail a dual-port MIMO antenna that integrates a T-shaped decoupling structure situated amidst its elements. This design effectively elevates the isolation level to above 24 dB. Further exploration in [10] introduces an alternative MIMO antenna design that incorporates polarization diversity and a unique docking floor strategy. This approach not only achieves an enhanced average isolation level exceeding 26 dB across the antenna's operational spectrum but also significantly expands its working bandwidth. The MIMO antenna with four ports described in [11] features a compact configura-

* Corresponding author: Gui Liu (iitgliu2@gmail.com).

tion, operating across a frequency spectrum of 3 to 13.5 GHz. Utilizing an orthogonal layout, this antenna demonstrates notably high isolation levels. The study presented in [12] introduces an antenna employing a neutralization line strategy to significantly diminish mutual coupling, thereby achieving an expansive impedance bandwidth of 96.47% within the range of 3.52–10.08 GHz. Nonetheless, the integration of various isolation techniques introduces complexities in both design and manufacturing processes. In [13], a dual-port MIMO antenna is operational at 3.1–10.6 GHz, and by incorporating a central slot etched into the ground, it achieves 31 dB superior isolation. The design proposed in [14] utilizes a $34 \times 34 \times 1.6\,\text{mm}^3$ FR4 substrate. Adjacent to the microstrip feed line, an electromagnetic bandgap (EBG) structure is included. This configuration facilitates triple-band slot behavior, extending the bandwidth from 2.5 to 12 GHz. Furthermore, while the EBG structure enhances the gain of antennas, the implementation of a frequency selection surface (FSS) technique is identified as a significant contributor to gain improvement. Ref. [15] describes the placement of an EBG structure adjacent to the antenna's feedline. The designed MIMO/diversity antenna has dimensions of $30 \times 44\,\text{mm}^2$. Furthermore, the design incorporated a hexagonal slot. Along with this, it featured F-shaped stubs. The purpose of these additions was to reduce mutual coupling. Ref. [16] presents a method for decreasing mutual coupling, which involves the use of a ground stub on the lower layer in conjunction with an EBG structure. This integrated approach effectively diminishes the coupling between radiation patches. In [17], a polarization diversity UWB antenna with a compact footprint of $25 \times 40\,\text{mm}^2$ is introduced. Its complexity arises from the use of two distinct ground planes. In [18], a 4-port UWB antenna is introduced. It boasts an impressive impedance bandwidth of 130.43%. This bandwidth spans from 2.8 to 13.3 GHz. This design employs orthogonally arranged rhombus-shaped monopoles to achieve polarization diversity and enhanced isolation, alongside an elliptical CSRR for notch band introduction. In [19], enhancements to voltage standing wave ratio (VSWR) bandwidth are suggested by changing the ground plane and adding an extended ground stub, which addresses modern automotive requirements. Additionally, a more extended ground stub was incorporated. Its purpose is to expand the bandwidth. This adaptation caters to the demands of modern automotive applications. A V-shaped monopole antenna is presented in [20]. It incorporates a staircase-shaped defective ground structure.

In summary, MIMO technology addresses some of the challenges faced by UWB systems, such as reliability issues and multipath fading. Adding various isolation technologies to MIMO antennas can achieve higher isolation and smaller size while maintaining antenna performance. Therefore, the integration of UWB technology and MIMO technology has attracted widespread attention and research interest from academia and industry. In recent years, numerous 4×4 UWB MIMO antennas with excellent performance have been proposed [21, 22]. However, in the UWB frequency, there are numerous narrowband communication systems, such as WLAN and 5G. These UWB and narrowband communication systems can interfere with each other, significantly impacting the performance of each system. Minimizing mutual interference between narrowband communication systems and UWB system signal has always been a research hotspot [23]. Although incorporating a band-stop filter in a UWB system can reduce interference, it introduces issues such as increased system complexity, larger size, and higher costs. Thus, it is essential to design a UWB antenna having a notch structure that can not only create the necessary notch in specific frequency bands but also resolve the frequency overlap issue between the UWB system and other wireless communication systems.

This paper presents a novel, small-size, easy-to-manufacture UWB antenna featuring dual-notch frequency band characteristics. The antenna can reduce mutual interference with 5G and WLAN systems. Moreover, its versatility allows for widespread use in civilian communications, providing stable and reliable wireless connections in homes, offices, and public spaces. In the medical field, its high efficiency enhances the accuracy and efficiency of remote diagnosis and treatment, significantly improving patients' treatment experiences.

The organization of this manuscript is outlined as follows. Section 2 details the design process and simulation results for the antenna unit. Section 3 introduces the designed MIMO antenna, which is based on the antenna unit. Additionally, the section presents both simulation and experimental results to facilitate a comparative analysis, thereby validating the performance of the antenna. Section 4 provides a summary of the paper.

2. SINGLE-PORT ANTENNA

Figure 1 depicts the specific geometry of the designed single-port antenna, which includes a coplanar waveguide ground plane, a microstrip feeder line, and a radiating element, all of which are manufactured on a 1.6-millimeter-thick FR4 dielectric substrate. Table 1 shows the detailed optimized parameters. The radiating element features a semi-circular metal patch incorporating a rectangular slot, a T-shaped strip and an inverted T-shaped strip, both of which are printed within the rectangular slot. Adjusting their sizes facilitates the acquisition of the desired notch frequency range, specifically 3.3–3.8 GHz.

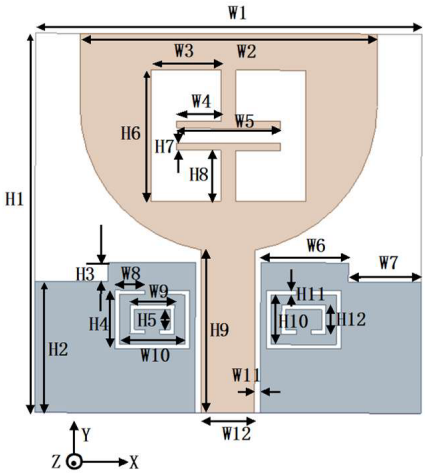

FIGURE 1. Geometry of the proposed single-port UWB antenna.

TABLE 1. The detailed optimized sizes (unit: mm).

Parameter	$W1$	$W2$	$W3$	$W4$	$W5$	$W6$
Value	26	20	4.7	3	7	5.9
Parameter	$W7$	$W8$	$W9$	$W10$	$W11$	$W12$
Value	5.8	2	3	4.4	0.4	3.6
Parameter	$H1$	$H2$	$H3$	$H4$	$H5$	$H6$
Value	26	9	1.3	4	1.4	9
Parameter	$H7$	$H8$	$H9$	$H10$	$H11$	$H12$
Value	0.5	3.5	11	3.4	0.3	2

Each of the coplanar waveguide ground planes has a rectangular complementary split resonant ring (CSRR) slot, which is symmetrical. By adjusting the sizes of the CSRR slots, the antenna can generate a notch frequency band ranging from 4.8 GHz to 6.0 GHz.

Figure 2 illustrates the shapes of a single-port ultra-wideband antenna at four different stages of the design process, named antenna-1, antenna-2, antenna-3, and antenna-4. The corresponding simulation results, demonstrating the reflection coefficient (S_{11}) for the single-port antenna across various configurations, are presented in Fig. 3.

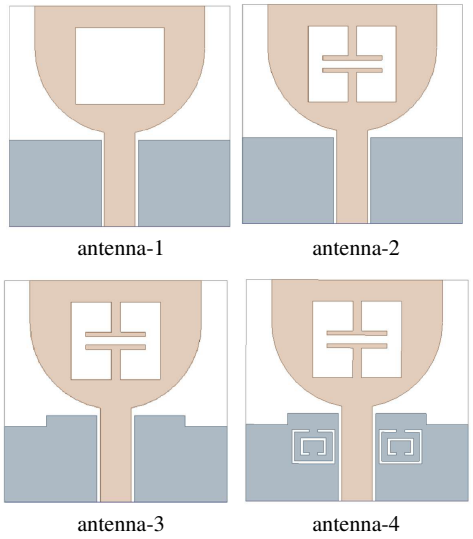

FIGURE 2. Design evolution of the single-port UWB antenna.

The radiating element of antenna-1 is a semi-circular metal patch with a rectangular slot, and the ground plane is a coplanar waveguide plane. Antenna-2 incorporates a double T-shaped filter structure based on antenna-1, establishing frequency exclusion zones in the range of 3.3 GHz to 3.8 GHz. The ground planes on both sides of antenna-2 are each cut by a rectangular strip, resulting in the shape known as antenna-3. Antenna-3 achieves a lower S_{11} within the frequency range of 7.0–11.0 GHz in comparison with antenna-2. Antenna-4, which features a CSRR structure, can generate a notched band ranging from 4.8 GHz to 6.0 GHz.

To better understand the functions of the T-shaped and inverted T-shaped filter structures and the CSRR slot, Fig. 4 provides the current distributions for the two suppression bands.

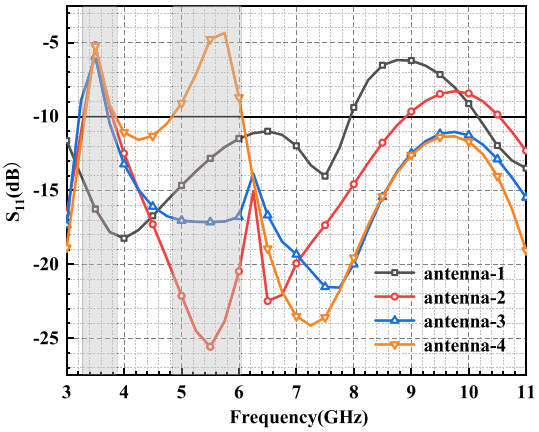

FIGURE 3. The simulated S_{11} parameters for antenna-1, antenna-2, antenna-3, and antenna-4.

Fig. 4(a) shows the current distribution at 3.5 GHz, which is primarily concentrated near the T-shaped and inverted T-shaped filter structures and is closely related to the 3.3–3.8 GHz frequency band. Fig. 4(b) illustrates the current distribution at 5.6 GHz. In this case, the rectangular CSRR slot significantly affects the surface current distribution. Therefore, the rectangular CSRR slot can effectively suppress the WLAN frequency band.

3. FOUR-PORT ANTENNA

Figure 5 presents the geometry of the designed MIMO antenna, which evolves from the aforementioned single port antenna and exhibits excellent isolation. The CSRR slots' locations on all rectangular metal ground planes of the MIMO antenna have been optimized and shifted 0.3 mm toward the radiation unit.

The final dimensions of the designed MIMO antenna are as follows: $W13 = 60$ mm, $W14 = 2$ mm, $W15 = 5$ mm, $W16 = 27$ mm, $H13 = 60$ mm, $H14 = 1$ mm, and $H15 = 2$ mm.

To further clarify the effect of the T-shaped filter structure on the notch, different values of *H15* and *H8* have been investigated and plotted in Fig. 6 and Fig. 7. Decreasing the values of *H15* causes an increase in the center frequency within the notch band. Changing the values of *H8* affects whether the first notch band exists. Finally, $H15 = 2$ mm and $H8 = 3.5$ mm are selected as the optimal dimensions for the T-shaped filter structure.

The overhead view of the manufactured prototype is illustrated in Fig. 8(a), while the underside view is illustrated in Fig. 8(b). Furthermore, Fig. 8(c) displays the measurement setup. Fig. 9 summarizes the S-parameter results, including both simulated and measured values. The antenna, as designed, functions across a frequency spectrum of 3.0 to 11.0 GHz. It includes frequency exclusion zones at 3.3–4.2 GHz and 4.8–6.0 GHz, with isolation exceeding 17 dB. The simulation results agree with the measurement.

Figure 10 shows the measured antenna radiation pattern. While the measurement is being conducted, one port is excited while the others are configured to match with 50-Ω load termi-

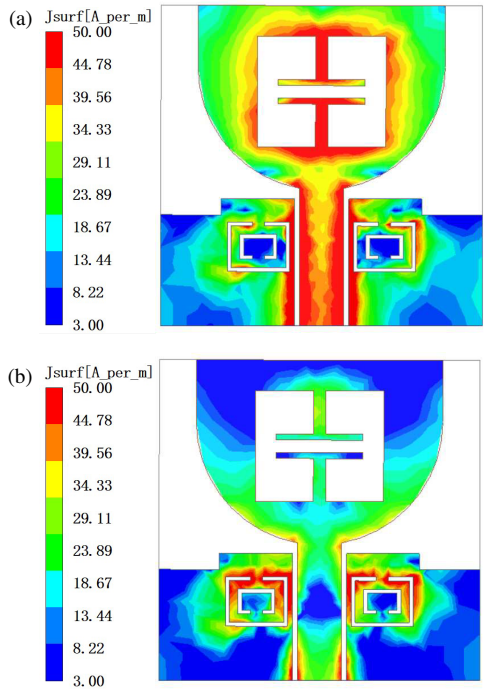

FIGURE 4. The current distribution of the single-port UWB antenna at (a) 3.5 GHz, (b) 5.6 GHz.

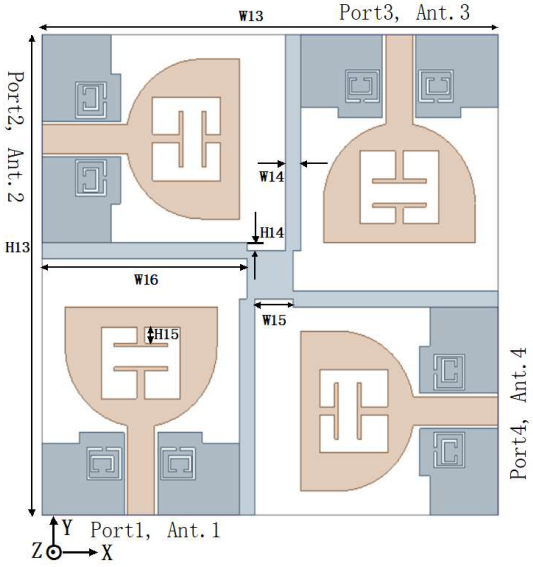

FIGURE 5. The geometry of the proposed 4 × 4 UWB MIMO antenna.

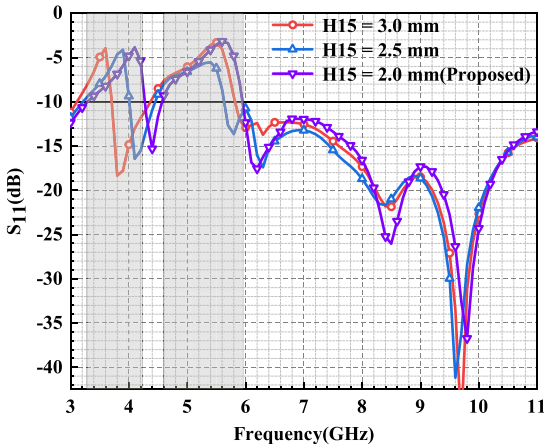

FIGURE 6. Simulated S_{11} of the proposed 4 × 4 UWB MIMO antenna with different values of $H15$.

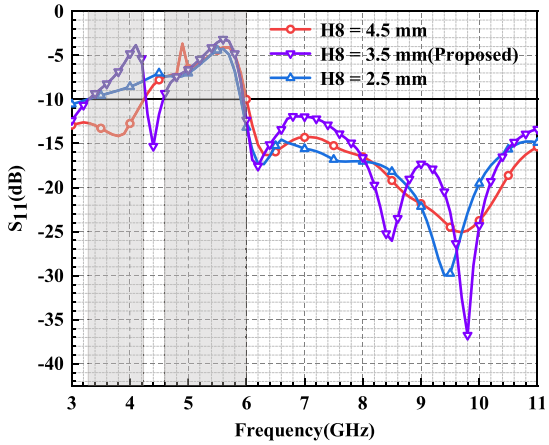

FIGURE 7. Simulated S_{11} of the proposed 4 × 4 UWB MIMO antenna with different values of $H8$.

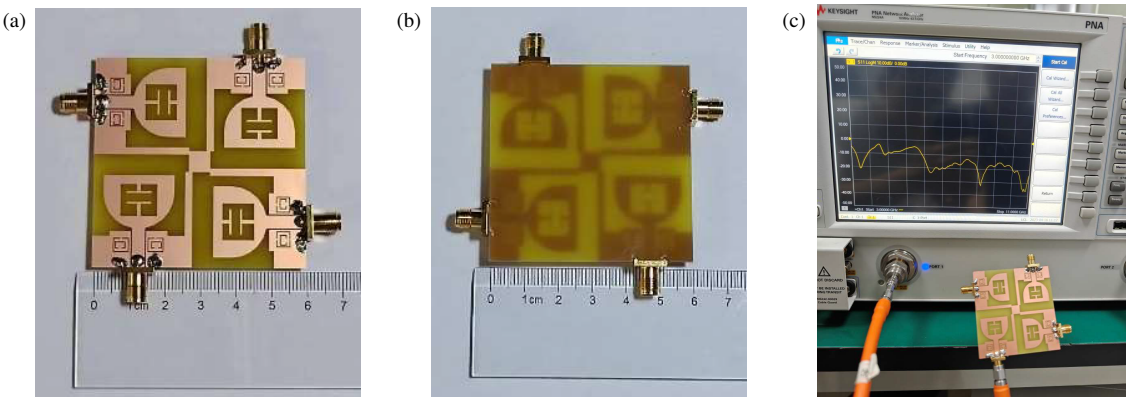

FIGURE 8. Photograph of the antenna prototype and measurement setup, (a) top view, (b) bottom view, (c) measurement setup.

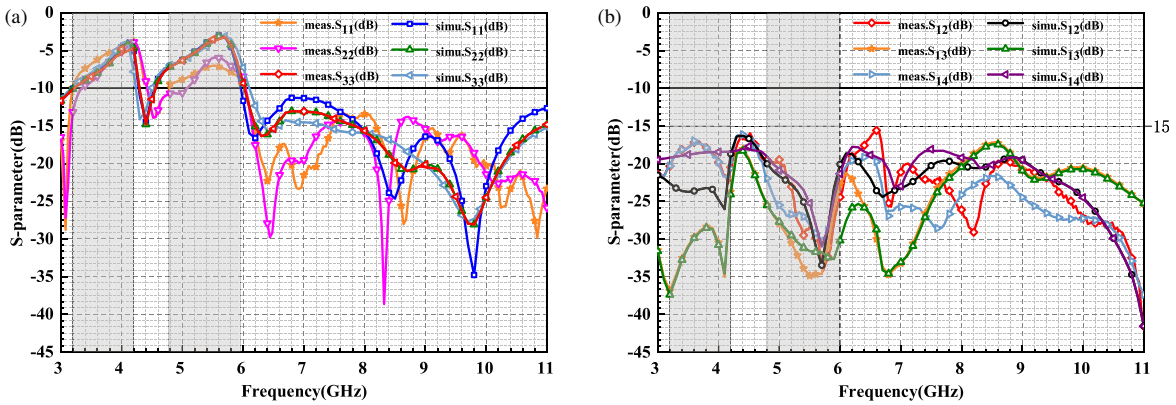

FIGURE 9. The simulated and measured S-parameters of the proposed 4×4 UWB MIMO antenna, (a) reflection coefficients, (b) transmission coefficients.

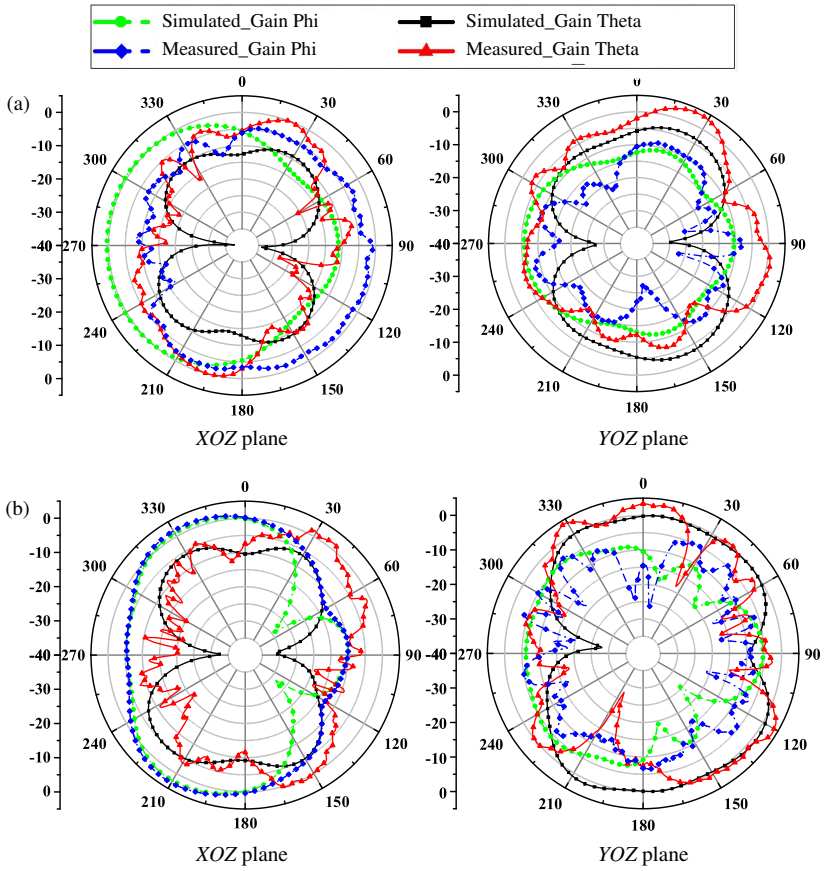

FIGURE 10. Radiation patterns of the proposed 4×4 UWB MIMO antenna, (a) 4.4 GHz, (b) 9.4 GHz.

nals. Fig. 11 presents a photograph of the manufactured antenna undergoing testing in an anechoic chamber.

The four elements in the MIMO antenna have the same size and configuration. Fig. 12 illustrates the gain and efficiency for just one element. Gain serves as a valuable metric for analyzing directional energy emission from antennas and evaluating fluctuations in radiation energy. The peak realized gain varies between 1.2 dB and 1.6 dB within the 4.2–4.8 GHz, and varies between 2.9 dB and 6.4 dB within the 6.0–11.0 GHz. Within the operational band of the antenna, the efficiency values are between 70.7% and 92.4%, with a peak efficiency of 92.4% at 7.0 GHz. In the notch band, both gain and efficiency decline significantly. The gain reaches a minimum of -1.5 dB at 5.6 GHz, and the efficiency drops to 45% at 5.7 GHz. In the transition bands near 3.3 GHz, 4.8 GHz, and 6 GHz, the performance of gain and efficiency is close to that of the 4.2–4.8 GHz band. The 4.2–4.8 GHz band can be used in short-distance communication scenarios where the requirements for gain and efficiency are not extremely high. Since the gain and efficiency within the 6–11 GHz frequency band are notably higher and relatively stable, this frequency band can be employed for practical UWB applications.

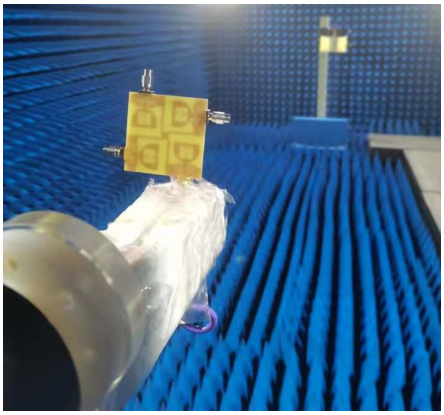

FIGURE 11. Testing in an anechoic chamber.

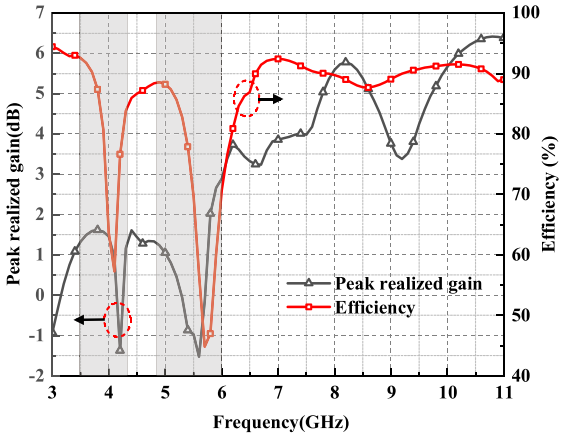

FIGURE 12. Measured efficiency and gain of the presented 4×4 UWB MIMO antenna.

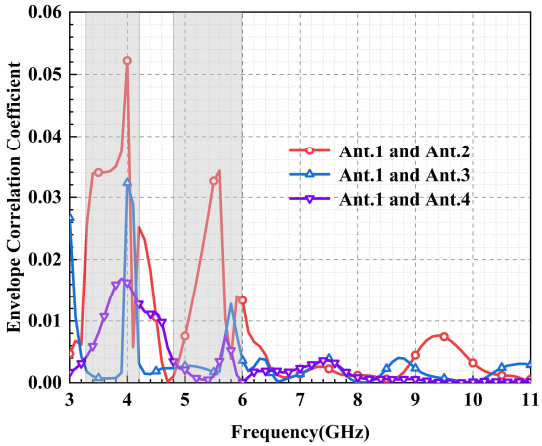

FIGURE 13. ECC of the presented 4×4 UWB MIMO antenna.

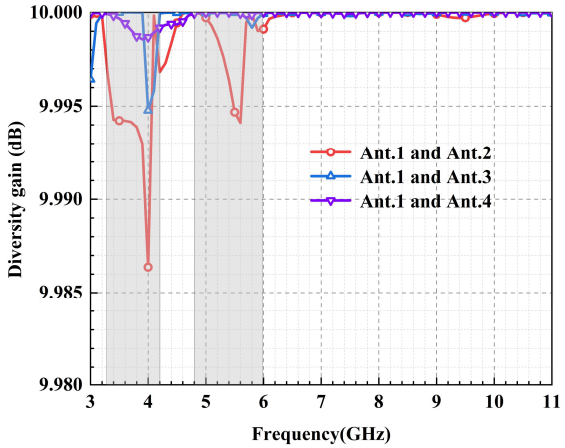

FIGURE 14. DG of the presented 4×4 UWB MIMO antenna.

ECC is a fundamental diversity parameter used to measure the signal correlation between different antennas in a MIMO antenna array. Low ECC values indicate good signal independence between antennas. The ECC consistently remains below 0.03 within the 4.2–4.8 GHz and 6.0–11.0 GHz frequency range, as illustrated in Fig. 13, and it is calculated using Equation (1) [29].

$$\mathrm{ECC} = \frac{\left|\iint_{4\pi}\left[\vec{F}_1(\theta,\phi) * \vec{F}_2(\theta,\phi)\right] d\Omega\right|}{\iint_{4\pi}\left|\vec{F}_1(\theta,\phi)\right|^2 d\Omega \iint_{4\pi}\left|\vec{F}_1(\theta,\phi)\right|^2 d\Omega} \tag{1}$$

Diversity Gain (DG) represents the gain achieved by using multiple antennas to enhance signal diversity in a multipath fading environment. A high DG value indicates superior system performance. The calculation formula for DG is shown in (2), and the results are shown in Fig. 14. The DG values exceed 9.985 dB.

$$\mathrm{DG} = 10\ (\mathrm{dB}) \times \sqrt{1 - |\mathrm{ECC}|^2} \tag{2}$$

Total Active Reflection Coefficient (TARC) is a measure of the effective operating bandwidth when multiple antennas are excited simultaneously. Low TARC values indicate good performance. TARC is calculated using the same formula as in [29], as shown in (3). The results are shown in Fig. 15 and achieve good performance of less than -10 dB.

$$\mathrm{TARC} = \sqrt{\frac{\left(S_{ii} + S_{ij}^*\right)^2 + \left(S_{ji} + S_{jj}^*\right)^2}{2}} \tag{3}$$

Mean Effective Gain (MEG) is an important parameter to measure the average receiving capability of a MIMO antenna in a specific environment. The value of MEG is considered below -3 dB [30]. The calculation formula of MEG is shown in (4), and the result is presented in Fig 16.

$$\mathrm{MEG}_i = \frac{1 - \sum_{j=1}^{k}\left(S_{ij}\right)^2}{2} \tag{4}$$

Group delay can be used to evaluate the signal transmission quality of ultra-wideband antennas. Fig. 17 shows the group delay of the proposed 4×4 UWB MIMO antenna. The group delay of the antenna is less than 1 ns within the operating frequency band. In addition, the group delay of the antenna has good flatness.

TABLE 2. Comparison among the proposed UWB MIMO antenna and other relevant designs.

Ref.	Port/s	Bandwidth (GHz)	Notch bands (GHz)	Gain (dB)	Efficiency (%)	ECC	Area (mm × mm)
[10]	4	2.1–20	3.3–4.1 8.2–8.6	5.8	> 80	< 0.02	80 × 80
[24]	4	3.0–16.2	4.0–5.2	3.0–8.0	> 75	< 0.3	60 × 60
[25]	4	3.38–10.56	3.52–4.22 5.23–6 7.29–8.2	−7–4	87.5–94.5	< 0.49	79.8 × 79.8
[26]	4	3.2–11.2	-	3–7.3	83–95	< 0.004	70 × 70
[27]	4	2.54–10.69	2.81–3.85 5.11–5.98 7.34–8.69	3.6–6.87	-	< 0.05	65 × 65
[28]	4	3.6–8.25	3.68–5.28 7.2–8.2	2.5–4.8	> 86	< 0.01	65 × 65
This work	4	3.0–11.0	3.3–4.2 4.8–6.0	1.2–6.4	70.7–92.4	< 0.03	60 × 60

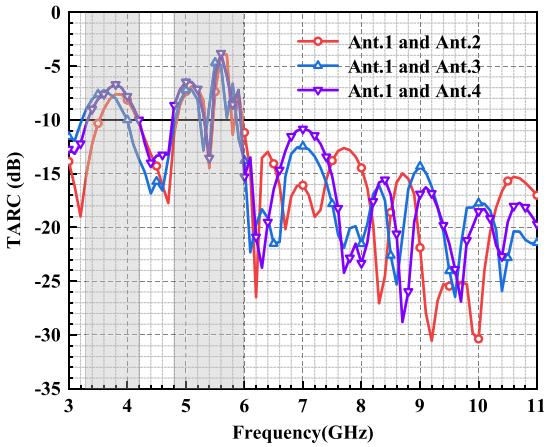

FIGURE 15. TARC of the presented 4 × 4 UWB MIMO antenna.

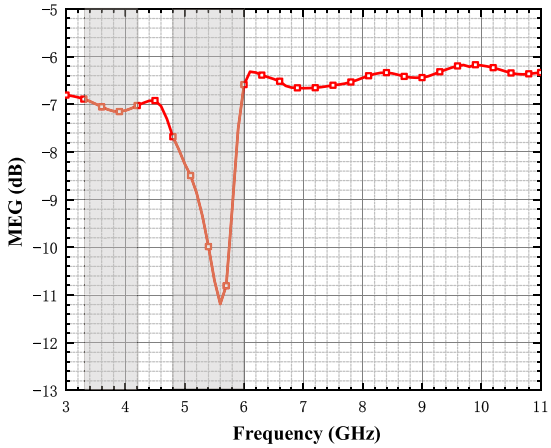

FIGURE 16. MEG of the presented 4 × 4 UWB MIMO antenna.

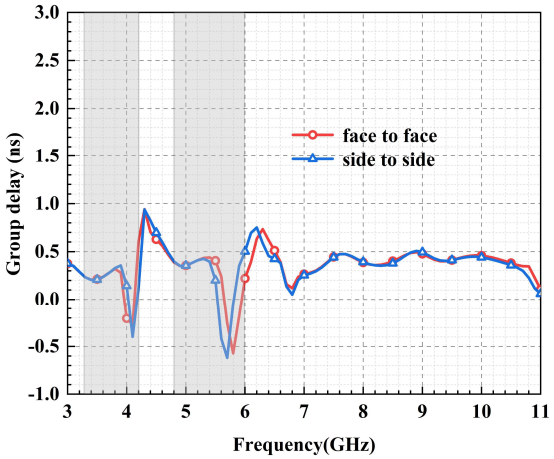

FIGURE 17. Group delay of the presented 4 × 4 UWB MIMO antenna.

Table 2 compares the bandwidth, notch bands, gain, efficiency, ECC, and area of the designed UWB antenna with those of six other presented antennas. Within the operational band of the designed antenna, the efficiency value is between 70.7% and 92.4% and the ECC below 0.03. The outcomes demonstrate that the antenna possesses superior performance.

4. CONCLUSION

In this paper, an antenna with dual-notch suppression for 5G and WLAN frequency bands is designed. The compact dimensions of the MIMO antenna are $60 \times 60 \times 1.6\,\text{mm}^3$. The antenna demonstrates $S_{11} < -10\,\text{dB}$ and isolation exceeding 17 dB. The peak realized gain varies between 1.2 dB and 1.6 dB within 4.2–4.8 GHz, and varies between 2.9 dB and 6.4 dB within 6.0–11.0 GHz. Additionally, the designed 4 × 4 UWB MIMO antenna achieves an ECC value lower than 0.03 and an efficiency value between 70.7% and 92.4% within the operating frequency band. The DG values exceed 9.985 dB, while the value of MEG is below −3 dB.

ACKNOWLEDGEMENT

The authors would like to acknowledge the Science and Technology Department of Zhejiang Province under Grant No. LGG19F010009, the National Natural Science Foundation of China under Grant No. 61671330, and Wenzhou Municipal Science and Technology Program under Grant No. C20170005 and No. 2018ZG019.

REFERENCES

[1] Bahmanzadeh, F. and F. Mohajeri, "Simulation and fabrication of a high-isolation very compact MIMO antenna for ultra-wide band applications with dual band-notched characteristics," *AEU — International Journal of Electronics and Communications*, Vol. 128, 153505, 2021.

[2] Li, R., L. Qu, and H. Kim, "A compact MIMO antenna design using the wideband ground-radiation technique for 5G terminals," *Journal of Electromagnetic Engineering and Science*, Vol. 24, No. 1, 89–97, 2024.

[3] Gorokhov, A., D. A. Gore, and A. J. Paulraj, "Receive antenna selection for MIMO spatial multiplexing: Theory and algorithms," *IEEE Transactions on Signal Processing*, Vol. 51, No. 11, 2796–2807, 2003.

[4] Abdulkawi, W. M., W. A. Malik, S. U. Rehman, A. Aziz, A. F. A. Sheta, and M. A. Alkanhal, "Design of a compact dual-band MIMO antenna system with high-diversity gain performance in both frequency bands," *Micromachines*, Vol. 12, No. 4, 383, 2021.

[5] Mandloi, M. S., P. Gupta, A. Parmar, P. Malviya, and L. Malviya, "Beamforming MIMO array antenna for 5G-millimeter-wave application," *Wireless Personal Communications*, Vol. 129, No. 1, 153–172, 2023.

[6] Tan, W. and S. Ma, "Antenna array topologies for mmWave massive MIMO systems: Spectral efficiency analysis," *IEEE Transactions on Vehicular Technology*, Vol. 71, No. 12, 12 901–12 915, 2022.

[7] Nassar, M. A., H. Y. Soliman, R. M. Abdallah, and E. A. F. Abdallah, "Improving mutual coupling in MIMO antennas using different techniques," *Progress In Electromagnetics Research C*, Vol. 133, 81–95, 2023.

[8] Pandurangan, D. and N. Mishra, "Various mutual coupling reduction techniques for 5G: MIMO antenna," in *Microwave Devices and Circuits for Advanced Wireless Communication*, 37–63, CRC Press, 2024.

[9] Kumar, A., A. Q. Ansari, B. K. Kanaujia, and J. Kishor, "A novel ITI-shaped isolation structure placed between two-port CPW-fed dual-band MIMO antenna for high isolation," *AEU — International Journal of Electronics and Communications*, Vol. 104, 35–43, 2019.

[10] Rekha, V. S. D., P. Pardhasaradhi, B. T. P. Madhav, and Y. U. Devi, "Dual band notched orthogonal 4-element MIMO antenna with isolation for UWB applications," *IEEE Access*, Vol. 8, 145 871–145 880, 2020.

[11] Khan, A. A., S. A. Naqvi, M. S. Khan, and B. Ijaz, "Quad port miniaturized MIMO antenna for UWB 11 GHz and 13 GHz frequency bands," *AEU — International Journal of Electronics and Communications*, Vol. 131, 153618, 2021.

[12] Tiwari, R. N., P. Singh, B. K. Kanaujia, and K. Srivastava, "Neutralization technique based two and four port high isolation MIMO antennas for UWB communication," *AEU — International Journal of Electronics and Communications*, Vol. 110, 152828, 2019.

[13] Radhi, A. H., R. Nilavalan, Y. Wang, H. S. Al-Raweshidy, A. A. Eltokhy, and N. A. Aziz, "Mutual coupling reduction with a wideband planar decoupling structure for UWB-MIMO antennas," *International Journal of Microwave and Wireless Technologies*, Vol. 10, No. 10, 1143–1154, 2018.

[14] Chen, Z., W. Zhou, and J. Hong, "A miniaturized MIMO antenna with triple band-notched characteristics for UWB applications," *IEEE Access*, Vol. 9, 63 646–63 655, 2021.

[15] Dalal, P. and S. K. Dhull, "Design of triple band-notched UWB MIMO/diversity antenna using triple bandgap EBG structure," *Progress In Electromagnetics Research C*, Vol. 113, 197–209, 2021.

[16] Khan, A., S. Bashir, S. Ghafoor, and K. K. Qureshi, "Mutual coupling reduction using ground stub and EBG in a compact wideband MIMO-antenna," *IEEE Access*, Vol. 9, 40 972–40 979, 2021.

[17] Zhang, S., B. K. Lau, A. Sunesson, and S. He, "Closely-packed UWB MIMO/diversity antenna with different patterns and polarizations for USB dongle applications," *IEEE Transactions on Antennas and Propagation*, Vol. 60, No. 9, 4372–4380, 2012.

[18] Kumar, S., G. H. Lee, D. H. Kim, W. Mohyuddin, H. C. Choi, and K. W. Kim, "Multiple-input-multiple-output/diversity antenna with dual band-notched characteristics for ultra-wideband applications," *Microwave and Optical Technology Letters*, Vol. 62, No. 1, 336–345, 2020.

[19] Alsath, M. G. N. and M. Kanagasabai, "Compact UWB monopole antenna for automotive communications," *IEEE Transactions on Antennas and Propagation*, Vol. 63, No. 9, 4204–4208, 2015.

[20] Jan, N. A., S. H. Kiani, F. Muhammad, D. A. Sehrai, A. Iqbal, M. Tufail, and S. Kim, "V-shaped monopole antenna with chichena itzia inspired defected ground structure for UWB applications," *Computers, Materials & Continua*, Vol. 65, No. 1, 19–32, 2020.

[21] Ren, W., Z. Wang, M. Yang, J. Zhou, and W. Nie, "Design of a simple four-port UWB-MIMO antenna based on a fan-shaped isolator," *Progress In Electromagnetics Research M*, Vol. 126, 117–126, 2024.

[22] Jhunjhunwala, V. K., P. Kumar, A. P. Parameswaran, P. R. Mane, O. P. Kumar, T. Ali, S. Pathan, S. Vincent, and P. Kumar, "A four port flexible UWB MIMO antenna with enhanced isolation for wearable applications," *Results in Engineering*, Vol. 24, 103147, 2024.

[23] Xiong, H., "An efficient narrowband interference suppression approach in ultra-wideband receiver," *IEEE Sensors Journal*, Vol. 17, No. 9, 2741–2748, 2017.

[24] Wu, W., B. Yuan, and A. Wu, "A quad-element UWB-MIMO antenna with band-notch and reduced mutual coupling based on EBG structures," *International Journal of Antennas and Propagation*, Vol. 2018, No. 1, 8490740, 2018.

[25] Jayant, S. and G. Srivastava, "Close-packed quad-element triple-band-notched UWB MIMO antenna with upgrading capability," *IEEE Transactions on Antennas and Propagation*, Vol. 71, No. 1, 353–360, 2023.

[26] Yao, Y., Y. Shao, J. Zhang, and J. Zhang, "A transparent antenna using metal mesh for UWB MIMO applications," *IEEE Transactions on Antennas and Propagation*, Vol. 71, No. 5, 3836–3844, 2023.

[27] Azimov, U. F., A. Abbas, S.-W. Park, N. Hussain, and N. Kim, "A 4-port flexible MIMO antenna with isolation enhancement for wireless IoT applications," *Heliyon*, Vol. 10, No. 11, 2024.

[28] Liu, L. Y., P. R. Zhang, A. K. Poddar, U. L. Rohde, and M. S. Tong, "A four-element ultra-wideband MIMO antenna with high

isolation for IOT applications," in *2024 Photonics & Electromagnetics Research Symposium (PIERS)*, 1–7, Chengdu, China, 2024.

[29] Yao, S., X. Qiu, and T. Yang, "A miniaturized UWB MIMO antenna design for 5G multi-band applications," *Progress In Electromagnetics Research C*, Vol. 153, 1–12, 2025.

[30] Jadhav, M. R. and U. L. Bombale, "Design of F-shaped parasitic MIMO antenna with DGS for vehicle-to-everything communication," *Progress In Electromagnetics Research B*, Vol. 109, 41–56, 2024.